Research on Chemical Intermediates (2022) 48:2721–2744
https://doi.org/10.1007/s11164-022-04711-y

Improved adsorption and desorption behavior of Cd on thiol-modified bentonite grafted with cysteamine hydrochloride

Ruiming Song[1] · Zhimei Li[1] · Wanli Li[1] · Ya An[1] · Mei Li[1] · Haoli Qin[1] · Chengshuai Liu[2]

Received: 23 December 2021 / Accepted: 21 March 2022 / Published online: 13 April 2022

Abstract

Clay adsorbents are considered an inexpensive and readily available solution for removing heavy metals, including cadmium, from the environment to reduce pollution. In this study, thiol-modified bentonite (SH-Bent) was prepared by grafting cysteamine hydrochloride onto natural bentonite (Bent). The effects of pH, equilibrium contact time, and temperature on the adsorption–desorption behavior of Cd^{2+} were studied, and adsorption isotherm models were applied to examine the adsorption behavior of SH-bent. SH-Bent demonstrated better performance and stability for Cd^{2+} adsorption than Bent. SH-Bent exhibited an enhanced adsorption capacity for Cd^{2+} at equilibrium of 49.3 mg/g at pH 6, 120 min, and 303 K, which was 42-fold higher than that of Bent under the same conditions. An investigation of the desorption behavior of Cd^{2+} adsorbed on Bent and SH-Bent in simulated acid rain revealed that SH-Bent has high stability, with a desorption rate of 5.73% at pH 4.5, 60 min, and 303 K, which was much lower than that demonstrated by Bent under the same conditions (45.68%). The Langmuir equation was the best-fitted adsorption isotherm model, closely followed by the Freundlich, Tempkin, and Dubinin–Radushkevich models. A significant difference in diffusion was observed between the two types of clay according to the intraparticle diffusion model. The adsorption–desorption processes of SH-Bent and Bent fit the pseudo-second-order model best among the five kinetic models examined. The information provided in this study can be used to apply thiol-modified clay for wastewater treatment or for the removal of cadmium from soil.

✉ Haoli Qin
hollyqin@126.com

Chengshuai Liu
liuchengshuai@vip.gyig.ac.can

[1] School of Chemistry and Materials Science, Guizhou Normal University, Guiyang 550025, China

[2] Institute of Geochemistry, Chinese Academy of Sciences, Guiyang 550081, China

Graphical abstract

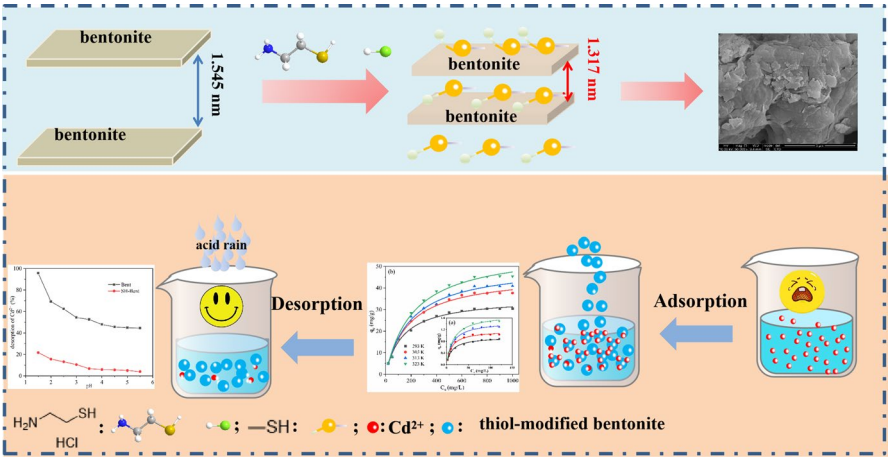

Keywords Modified bentonite · Cadmium · Adsorption · Desorption · Isotherm · Kinetics

Abbreviations

q_e	Adsorption capacity at equilibrium (mg/g)
q_t	Amount of Cd^{2+} adsorbed per unit mass of adsorbent at any time t (mg/g)
Q_e	Amount of Cd^{2+} desorption per unit mass of adsorbent at any time t (mg/g)
C_e	Equilibrium concentration of Cd^{2+} in solution (mg/L)
C_0	Initial concentration of the Cd^{2+} solution (mg/L)
V	The volume of the Cd^{2+}solution (mL)
m	Amount of adsorbent used (g)
η_e	The percentage removal of Cd^{2+}
Q_m	Maximum adsorption at monolayer coverage (mg/g)
K_L	The intensity of adsorption (L/mg)
K_F	Freundlich isotherm constant related to adsorption capacity ((mg/g) (L/mg)1/n)
n_F	Freundlich isotherm constant related to adsorption intensity
A_T	Tempkin adsorption potential (L/mg)
B_T	Tempkin isotherm energy constant (dimensionless)
b_T	Tempkin heat of adsorption (kJ/mol)
ε	Polanyi potential
γ	D–R adsorption energy constant (mol^2/kJ^2)
K_2	The rate constant of second-order adsorption (g/mg min)
E	Adsorption energy (kJ/mol)
t	Time (min)
τ	Surface coverage (desorption constant).
a	Rate of chemisorption (initial adsorption rate)

R^2 Correlation coefficient
b Constant related to the extent of adsorption (L/mg)
R Gas constant (J/mol K)
T Absolute temperature (K)

Introduction

One of the fundamental challenges of this era is the fight to reduce pollution, including heavy metal pollution, in order to improve the natural environment. Heavy metal pollution mostly originates from industrial production, transportation, and domestic waste. In industrial production, most pollutants, such as nickel, copper, zinc, and cadmium, are eventually released into the environment [1]. Cadmium is the most toxic heavy metal in water [2]. It is a nonessential element for animals and plants. It cannot be biodegraded once it enters the human body, and instead leads to osteomalacia and renal failure [3]. Cadmium pollution mostly originates from electroplating, metallurgy, chemical manufacturing, and battery manufacturing. According to the Environmental Protection Bureau of China, the allowable limit for Cd^{2+} discharge into the environment is 0.1 mg/L. Methods to remove large quantities of cadmium are necessary to avoid significant harm to the environment when large quantities of cadmium are discharged.

Heavy metal removal methods include chemical precipitation, oxidation/reduction, membrane filtration, ion exchange, and adsorption [4]. Most of these treatments have disadvantages, such as high cost, low efficiency, the potential for secondary contamination, and incompatibility with pollutants [5]. Among these methods, adsorption is considered one of the most promising methods to remove heavy metals owing to its flexibility and simplicity and because it does not cause secondary contamination [6, 7]. Therefore, a large number of unconventional, inexpensive, and readily available adsorbents have been tested for the removal of heavy metals, including clay minerals [8, 9], biomaterials [10, 11], and industrial solid wastes [12]. In particular, clay minerals present distinct advantages for removing heavy metals because of their overwhelming abundance, high cation exchange capacity, low cost, simplicity, and environmental-friendliness [13].

Bentonite (Bent) is a 2:1 layered silicate clay mineral composed of two layers of silicon–oxygen tetrahedral sheets and a layer of aluminum (magnesium) oxygen octahedral sheets [14]. The interaction mechanism between Bent and metal ions relies on cation exchange caused by the structural negative charge (permanent) in the interlayer and the formation of complexes containing silanol or aluminol groups due to the edge surface charge (variable) [15]. However, because of the exchange and release of the adsorbed metals over the long term, Bent exhibits poor stabilization performance [16]. The adsorption capability of Bent can be improved by inserting organic groups and inorganic matter between the layers [17, 18]. Anirudhan et al. [19] reported the enhancement of tannin removal using cationic surfactant-modified bentonite. Liu et al. [20] reported that gemini surfactant-modified montmorillonite exhibited a favorable adsorption capacity for phenol and catechol. Ghiaci et al.

[21–23] found that CTMAB-modified bentonites effectively immobilized Candida rugosa lipase, alkaline phosphatase, and α-amylase.

As thiol groups can form stable complexes with metals, preferential chelation occurs according to Pearson's hard and soft acids and bases theory, which states that soft acids and soft bases chelate more easily. In recent years, several effective adsorbents for the removal of heavy metals, involving thiol-modified clay with dimercaprol [9] and 3-mercaptopropyltrimethoxysilane [24] as complexing agents, have been reported. Cysteamine hydrochloride has strong metal complexation properties, applied in the medical field as a pharmaceutical intermediate. However, it was first used successfully to modify Na-bentonite to remove Cr(VI) in our laboratory [25]. In this study, cysteamine hydrochloride will be carried out to modify natural Ca-bentonite to remove Cd(II). In addition, it is not only that the removal rate of heavy metals by adsorbents, but also that the problem of secondary pollution caused by releasing adsorped heavy metals to environment should be further studied, which was hardly mentioned in previous reports. So the stability of adsorbents after adsorption of heavy metals will be investigated in this study, which would provide a experience for the practical application of adsorbents in the environment.

In this study, a functional thiol-modified bentonite (SH-Bent) grafted by cysteamine hydrochloride, with improved removal performance and stability for Cd^{2+}, was evaluated using batch experiments and compared to raw clay minerals (Bent) in aqueous solutions. Detailed isotherm adsorption, kinetics, and acid rain desorption were carried out to explore the potential of SH-Bent to remove heavy metals, using Cd^{2+} as the representative heavy metal cationic species and clay minerals as adsorbents. A series of morphological and structural research methods was used to further analyze the adsorption characteristics and cadmium absorption mechanisms of Bent and SH-Bent.

Material and methods

Material and reagents

The clay used in this study was natural bentonite, collected from Chifeng, Inner Mongolia, China. The reagents used to modify Bent and for the adsorption tests, including cadmium chloride hemihydrate ($CdCl_2 \cdot 2.5H_2O$), hydrochloric acid (HCl), cysteamine hydrochloride, sodium hydroxide (NaOH), and sodium chloride (NaCl), were of analytical purity and were purchased from Aladdin Company. A fresh stock solution of Cd^{2+} was prepared by dissolving $CdCl_2 \cdot 2.5H_2O$ in deionized water. NaOH and HCl were used to adjust the pH.

Preparation of adsorbents

SH-Bent was prepared by grafting cysteamine hydrochloride onto Bent using the following procedure [25]: First, acidified bentonite (H-Bent) was prepared by mixing Bent with 20% HCl at a volume ratio of 1:10 and stirring in an 80 °C water bath

for 4 h. After activation, the Bent portions were separated from the solution by centrifugation and washed with distilled water several times until all Cl^- was removed, as visualized when a 0.01 M $AgNO_3$ droplet was deposited on the supernatant. The H-Bent was then dried at 110 °C for 6 h and ground. SH-Bent was prepared as follows: H-Bent powder was dispersed in deionized water to obtain a 2% suspension, which was then mixed with 10 g/L cysteamine hydrochloride at a volume ratio of 10:1 and stirred for 4 h. SH-Bent was centrifuged at 8000 rpm for 10 min, washed with deionized water several times, dried at 60 °C, and ground with a 200-mesh sieve.

Characterization of adsorbents

The functional groups of Bent and SH-Bent were characterized using Fourier transform infrared spectroscopy (FTIR). The wavenumber ranged from 4000 to 400 cm^{-1} with a resolution of 4 cm^{-1} (Bruker Tensor 27). The X-ray diffraction (XRD) patterns of the obtained Bent and SH-Bent were measured continuously at 40 kV and 30 mA from 2°–70° using a Bruker D8 Advance diffractometer with Cu-K α radiation. The morphologies of Bent and SH-Bent were investigated by scanning electron microscopy (SEM, FEI/INSPECT F50 US). The Brunauer–Emmett–Teller (BET) surface area and pore size distribution were measured using a Micromeritics ASAP 2460 analyzer. The adsorption data were analyzed using BET theory, and the pore size distribution was analyzed using non-local density functional theory, assuming a slit-pore geometry (MicroActive software from Micromeritics Instruments).

Adsorption–*desorption studies*

An appropriate quantity of $Cd{\cdot}2.5H_2O$ was dissolved in distilled water to form a stock solution of Cd^{2+} with a concentration of 5000 mg/L and an ionic strength of 0.1 M NaCl. The stock solution was diluted to obtain an initial Cd^{2+} concentration identical to that used in the adsorption experiment. For the equilibrium experiments, 0.15 g of each adsorbent was mixed with 30 mL Cd^{2+} solution at different initial concentrations. The experimental conditions, including pH, equilibrium contact time, and temperature, were optimized. Batch experiments were carried out with the adsorbent–supernatant in a 50-mL centrifuge tube at 30 °C and 200 rpm in an air bath constant-temperature oscillator. The influence of pH on Cd^{2+} adsorption was investigated. The pH of the Cd^{2+} solution was adjusted from 3 to 10 using 1 M HCl and 1 M NaOH solutions. The effect of temperature on the adsorption process was investigated by varying the temperature from 20 to 50 °C. The impact of different contact times on the Cd^{2+} adsorption process was examined. After each reaction, the clay was separated from the solution by centrifugation at 5000 rpm for a certain period. The concentration of residual cadmium in the supernatant was determined by ICP-OES (Agilent 5110).

In the desorption experiment, the suspension was centrifuged after adsorption of Cd^{2+}, and the Cd^{2+} loaded on the surface of Bent and SH-Bent was washed with deionized water to remove unabsorbed Cd^{2+}. Then, the samples were re-suspended

in a 50-mL centrifuge tube with 30 mL of simulated acid rain at pH 1.5 to 5.5, respectively. The equilibrium conditions were consistent with those of the adsorption process. The concentration of Cd^{2+} in the supernatant liquid was measured using ICP-OES (Agilent 5110). When preparing samples to simulate acid rain, only the major anion composition in acid rain was considered. The mixture was prepared with a molar ratio of H_2SO_4 and HNO_3 at 4:1 and then diluted with deionized water to form a simulated acid rain solution with a pH value of 1.5 to 5.5. The adsorption and desorption experiments were conducted in triplicate, and the standard deviations of the results were calculated. Isotherms were obtained under the optimized reaction conditions, and the kinetics of the adsorption process and those of acid rain desorption were studied.

Theory

Adsorption

The equilibrium adsorption quantity, q_e (mg/g), was calculated using the following formula:

$$q_e = \frac{(C_0 - C_e)V}{C_0} \tag{1}$$

and the removal rate of Cd^{2+} can be expressed as follows [26]:

$$\eta_e = \frac{C_0 - C_e}{C_0} \times 100\% \tag{2}$$

Adsorption isotherm models

In general, adsorption isotherms provide useful data for optimizing the use of adsorbents. For example, they describe the bond energy, affinity, and adsorption capacity of the adsorbents. The adsorption isotherm models examined in this study include the Langmuir, Freundlich, Tempkin, and Dubinin–Radushkevich isotherm models (Table 1). The experimental data were fitted into the above models to understand the adsorption mechanism, surface properties, and affinity of Bent and SH-Bent for Cd^{2+} removal.

Table 1 Adsorption isotherm models

Model	Langmuir model	Freundlich model	Tempkin model	Dubinin–Radushkevich model
Equation	$q_e = \frac{Q_m K_L C_e}{1+K_L C_e}$	$q_e = K_F (C_e)^{1/n_F}$	$q_e = B_T \ln A_T + B_T \ln C_e$	$\ln q_e = \ln Q_m - \gamma \varepsilon^2$

Adsorption–desorption kinetic models

An examination of the adsorption–desorption kinetics was necessary to determine the efficiency of the adsorbent and describe the adsorption and desorption rate, which determines the diffusion process and the adsorption and desorption time of the adsorbent at the solid–liquid interface. To define the adsorption and desorption rates and describe how Cd^{2+} migrated to the two clay surfaces, different kinetic models were used (Table 2).

Results and discussion

Characterization

FTIR spectra

Figure 1 shows the infrared spectra of Bent and SH-Bent in the range 400–4000 cm^{-1}. For the raw clay, the strong adsorption band at 3635 cm^{-1} is attributable to the stretching vibration of O–H functional groups in the octahedral structure [27], and the wide adsorption band at 3436 cm^{-1} represents the stretching vibration of water [28]. The peak at 1446 cm^{-1} corresponds to the bending vibration of the C–O–C groups. The peak of the medium-width adsorption band at 1641 cm^{-1} corresponds to the bending vibration of H_2O. The adsorption peak near 1039–1043 cm^{-1} represents the stretching vibration of the Si–O tetrahedron. The adsorption peak at 1082 cm^{-1} was attributed to the stretching vibration of Si–O amorphous silica. At 916 cm^{-1}, the bending vibration of the Al_2OH groups was observed [29]. The peak at 624 cm^{-1} represents coupled out of plane Al-O and Si–O [30]. The peaks at 521 $cm^{-1}$and 465 cm^{-1} were attributed to the bending vibrations of Si–O-Mg and Si–O-Fe, respectively [31]. After modification, three bands remained in the SH-Bent spectrum at 3635 cm^{-1}, 1039 cm^{-1}, and 1082 cm^{-1}, suggesting that the inherent lamellar structure of Bent was retained. Furthermore, the stretching vibration of C–O–C at 1446 cm^{-1} shifted to a lower wavenumber and weakened after modification, possibly due to acidification leading to the dissolution of $CaCO_3$. A weak peak is present at 2554 cm^{-1}, which could be a result of the stretching vibration of S–H, indicating that thiol groups were grafted onto the Bent [25].

XRD

XRD tests were used to investigate the changes in bentonite layer spacing before and after clay modification. The interlayer distance is given by [32] (Eq. 3):

$$2\mathrm{d}\sin\theta = n\lambda \tag{3}$$

where d corresponds to the interlayer distance, λ corresponds to the XRD wavelength, θ corresponds to the glancing angle, and $n = 1$.

Table 2 Adsorption–desorption kinetic models

Model	Pseudo-first-order	Pseudo-second-order	Elovich	Itraparticle diffusion	Two-constant
Equation	$\ln\left(q_e - q_t\right) = \ln q_e - K_1 t$	$\frac{t}{q_t} = \frac{1}{K_2 q_e^2} + \frac{t}{q_e}$	$q_t = \frac{1}{\tau}\ln\left(a\tau\right) + \frac{1}{\tau}\ln t$	$q_t = K_{\text{int}} t^{0.5}$	$q_t = at^b$

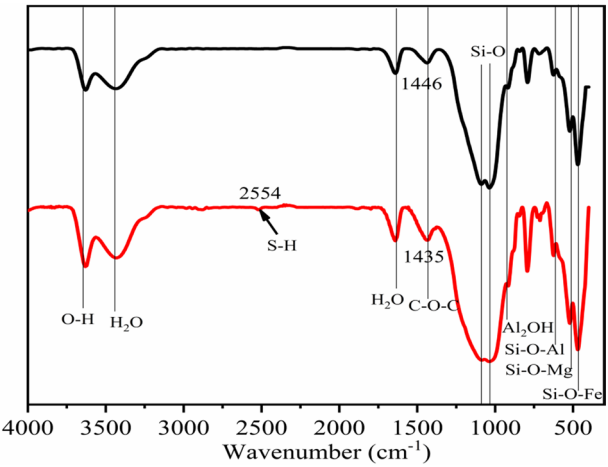

Fig. 1 FTIR spectra of Bent and SH-Bent

Figure 2 shows that the interlayer distance of Bent was calculated to be 1.545 nm. The 001 peak of the modified clay shifted to the right. The basal spacing was determined to be 1.317 nm, indicating that the thiol groups were adsorbed on the interlayer of bentonite, reducing the interlayer distances [33]. Additionally, the intensity of the 001 peak decreased after modification, possibly due to the addition of HCl to reduce the degree of crystallinity, and the surface became more heterogeneous [34]. Notably, the peak broadened significantly after modification, indicating that the adsorption of thiol groups leads to an increase in the crystal size [28].

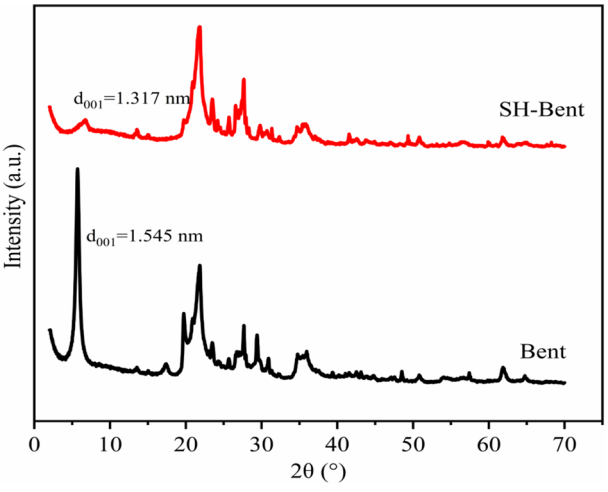

Fig. 2 XRD patterns of Bent and SH-Bent

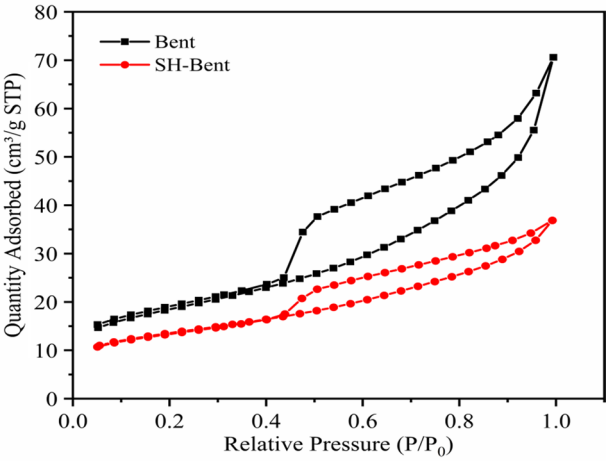

Fig. 3 N_2 adsorption/desorption isotherms on Bent and SH-Bent at 77 K

Table 3 BET results for Bent and SH-Bent

Sample	Surface area (m^2/g)	Average pore diameter (nm)	Pore volume (cm^3/g)
Bent	63.3	6.90	0.109
SH-Bent	45.5	5.01	0.057

BET

Figure 3 shows the adsorption–desorption isotherms of Bent and SH-Bent. According to the IUPAC classification system, the isotherms of the two adsorbents can be classified as type IV, which is typical for mesoporous materials. The addition of thiol groups did not significantly alter the pore shape. The hysteresis loop verifies the presence of evaporation and capillary condensation at a higher P/P_0, indicating the completion of mesopore filling [35]. In addition, for Bent, when the relative pressure (P/P_0) was approximately 0.43, the adsorption value of N_2 increased rapidly with increasing P/P_0, possibly due to the existence of mesopores or a small number of macropores [36]. As shown in Table 3, the BET surface area, total pore volume, and average pore diameter decreased significantly after modification. However, the volume of the micropores increased slightly. The decrease in the BET surface area was probably a result of the immobilized organic ligands that were embedded in the interlayer of Bent, blocking the pores [37]. The reduction in pore diameter and pore volume supports this hypothesis [33].

SEM

The morphologies of Bent and SH-Bent are shown in Fig. 4. In the Bent image, a rigid shape and small platelets were visible (Fig. 4a), whereas SH-Bent (Fig. 4b)

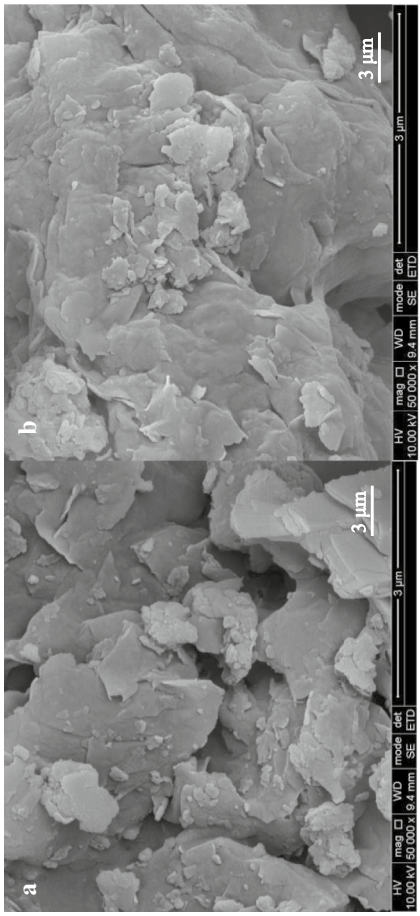

Fig. 4 SEM images of **a** Bent, **b** SH-Bent

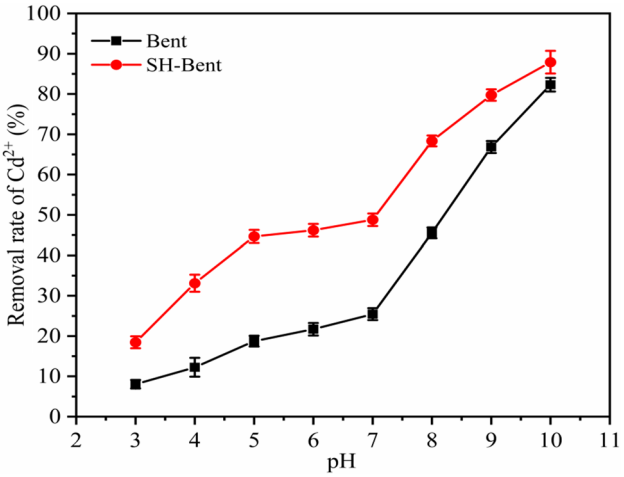

Fig. 5 Effect of initial pH for Cd^{2+} adsorption on Bent and SH-Bent (Cd^{2+} concentration, 20 mg/L; adsorbent dose, 5 g/L; temperature, 30 ± 0.1 °C; 200 rpm)

had a much smoother surface and tighter layered structures after modification. This result is consistent with the FTIR, XRD, and BET results. Owing to the intercalation of thiol groups into Bent, the SH-Bent layers appeared to be conjoined, thus reducing the interlayer distance and decreasing the surface area.

Adsorption results

Effect of initial pH values

The removal rate of Cd^{2+} by the two adsorbents increased with increasing pH. However, the SH-Bent removal capability of Cd^{2+} was significantly higher than that of Bent (Fig. 5). In the bentonite-aqueous system, the adsorption of Cd^{2+} by the adsorbent was mostly affected by the surface charge, which in turn depended on the reactivity of H^+ and OH^- with the bentonite surface. At very low pH, the quantity of H^+ exceeds that of Cd^{2+}, and competitive adsorption occurs at the binding sites on Bent and SH-Bent [38]. In addition, the thiol groups of SH-Bent are protonated, leading to electrostatic repulsion, and limiting their chelating ability. The concentration of H^+ decreases, which is attributed to an increase in pH, and the number of negatively charged sites increases, which is conducive to the adsorption of metal cations [39]. When the pH becomes alkaline, cadmium hydroxide precipitation occurs, which may increase the removal of Cd^{2+} from the solution.

The K_{SP} value of $Cd(OH)_2$ is 5.27×10^{-15} [40]. The pH for the precipitation of Cd^{2+} from a 20 mg/L solution was 8.74. However, considering experimental results reported by Kayoed [41], $Cd(OH)_2$ is expected to precipitate at pH values higher than 6. Therefore, we performed all adsorption experiments at pH 6.

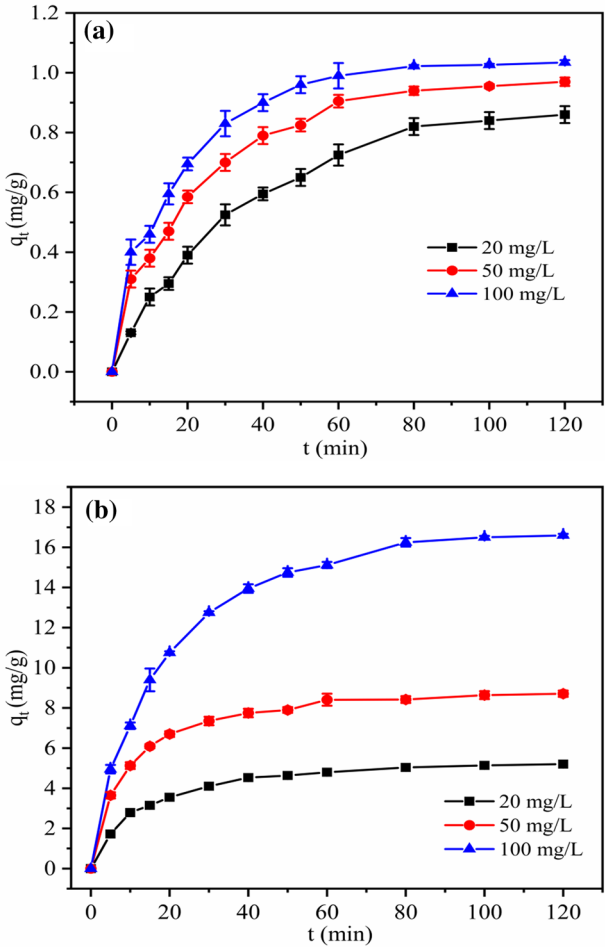

Fig. 6 Effect of contact time for Cd^{2+} adsorption on **a** Bent and **b** SH-Bent (Cd^{2+} concentration was 20, 50, 100 mg/L, respectively; adsorbent dose, 5 g/L; pH, 6.0 ± 0.1; temperature, 30 ± 0.1 °C; 200 rpm)

Effect of contact time

The adsorption process is a rapid physical–chemical reaction [42]. Based on this, the effects of Bent (Fig. 6a) and SH-Bent (Fig. 6b) on the adsorption of Cd^{2+} were studied using contact time experiments. The Cd^{2+} initial solute concentrations were 20, 50, and 100 mg/L. SH-Bent adsorbed rapidly in the first 20 min. As there are many adsorption sites in the initial stage, Cd^{2+} easily interacts with the adsorption sites of clay, while the slow adsorption rate in the later stage was attributed to the difficult diffusion of the solute into the interior adsorbent [20].

Furthermore, adsorption equilibrium was achieved within 80–120 min, probably because of the gradual occupation of the active sites. Therefore, a contact time of 120 min was selected for follow-up studies to ensure equilibrium adsorption.

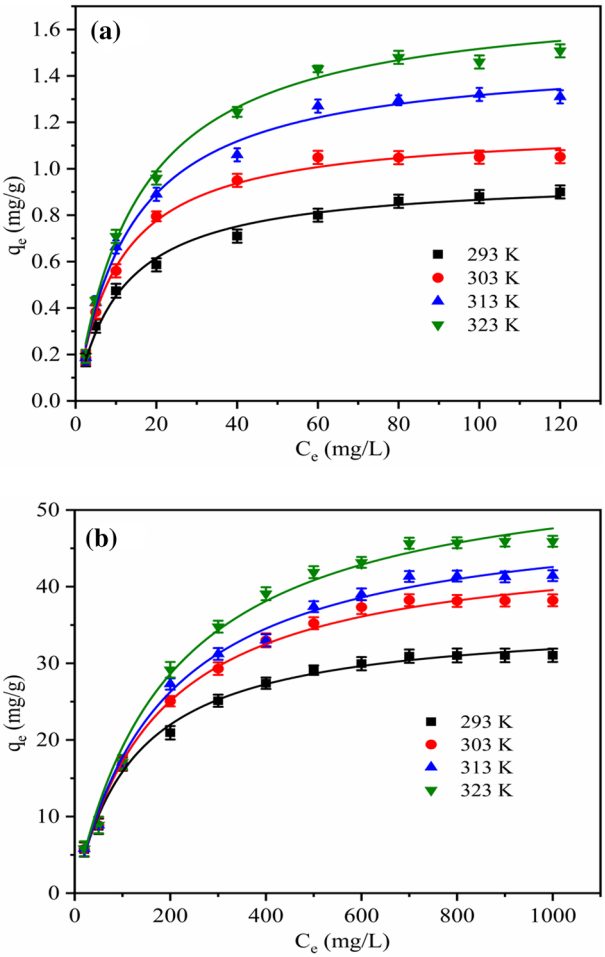

Fig. 7 Comparison of Cd^{2+} adsorption on **a** Bent and **b** SH-Bent with Langmuir adsorption isotherms (adsorbent dose, 5 g/L; pH, 6.0 ± 0.1; contact time, 120 min; temperature, 30 ± 0.1 °C; 200 rpm)

Figure 6 shows that the adsorption capacity of SH-Bent was much higher than that of Bent at all times. These characteristics indicate that SH-Bent is suitable for industrial wastewater treatment and can be applied in emergencies, such as leakage of contaminated water, metal ion pollution in groundwater, or other water pollution emergencies, which require a large adsorption capacity and fast adsorption.

Adsorption isotherm models

The maximum uptake of Cd^{2+} by Bent and SH-Bent at 293–323 K was determined when the Cd^{2+} concentration was 20–1000 mg/L (Fig. 7). Because adsorption

Table 4 Parameters of equilibrium isotherm models for Cd^{2+} adsorption on Bent and SH-Bent

Equilibrium models	Parameters	Bent				SH-Bent			
		Absolute temperature (K)							
		293	303	313	323	293	303	313	323
Langmuir isotherm	K_L(L/mg)	0.082	0.090	0.071	0.062	0.007	0.006	0.005	0.005
	q_m(mg/g)	0.951	1.169	1.479	1.731	35.58	49.30	50.73	57.81
	R^2	0.991	0.990	0.991	0.994	0.993	0.994	0.993	0.992
Freundlich isotherm	K_F(L/g)	0.193	0.257	0.268	0.282	3.011	2.774	2.637	2.668
	n_F	3.078	3.194	20,856	2.711	2.863	2.543	2.430	2.347
	R^2	0.954	0.911	0.919	0.923	0.923	0.930	0.938	0.929
Tempkin isotherm	b_T(KJ/mol)	12.95	10.80	8.613	7.521	0.338	0.265	0.250	0.226
	A_T	0.965	1.019	0.790	0.689	0.111	0.066	0.060	0.054
	R^2	0.981	0.964	0.985	0.989	0.979	0.978	0.979	0.974
D-R isotherm	q_m(mg/g)	0.691	0.887	1.063	1.193	24.79	29.45	31.16	34.17
	E(KJ/mol)	1.449	1.405	1.385	1.395	2.009	1.977	2.008	2.020
	R^2	0.805	0.869	0.869	0.849	0.684	0.649	0.639	0.622

isotherms are very important for depicting the adsorption behavior of Cd^{2+} and the maximum adsorption capacity of Cd^{2+} on Bent and SH-Bent, four adsorption models were used to depict the adsorption behavior of Cd^{2+} in this study.

Table 4 shows the relevant data for the Langmuir, Freundlich, Tempkin, and Dubinin–Radushkevich adsorption isotherms for the two adsorbents at $T = 293$, 303, 313, and 323 K, respectively. The correlation coefficients (R^2) range from 0.8 to 1.0, indicating extremely strong correlations. Thus, the adsorption of Cd^{2+} on SH-Bent at different temperatures conforms to three isotherm adsorption models, and that of Bent is consistent with four isotherm adsorption models. The R^2 value for the Freundlich model is less than 0.96. Moreover, the value of n_F was higher than unity, indicating that Cd^{2+} was favorably adsorbed by SH-Bent and Bent [43, 44]. The R^2 values for the Bent and SH-Bent models were all approximately 0.98. The value of b_T decreases with an increase in temperature, which implies that heating is beneficial for adsorption [45]. As the D-R isotherm did not fit the model for values lower than 0.7, it does not describe the removal of Cd^{2+} by SH-Bent when R^2 is lower than 0.7.

The R^2 value for the Langmuir model was the highest among those of the four adsorption isotherm models, indicating that it represented the adsorption process best. The adsorption process occurs at specific homogeneous surface-active sites of Bent and SH-Bent, which may exhibit monolayer binding. According to the Langmuir adsorption model, the adsorption q_m values of Cd^{2+} on Bent and SH-Bent were the highest at $T = 323$ K and the lowest at $T = 293$ K, implying that the adsorption capacity increased with temperature. Moreover, the q_m value of SH-Bent was 49.30 mg/g at 303 K, which was more than 42 times the adsorption capacity of Bent. This may be a result of the dissolution of part of the tetrahedron and octahedron sheets, resulting in Cd^{2+} filling the micropores of SH-Bent or the

Table 5 Parameters of kinetic model parameters for the adsorption of Cd^{2+} on Bent and SH-Bent

Kinetic models	Parameters	Bent			SH-Bent		
		Concentration of Cd^{2+}solution (mg/L)					
		20	50	100	20	50	100
Pseudo-first-order	q_e(mg/g)	0.857	0.926	0.988	3.483	8.036	15.95
	K_1	0.027	0.049	0.053	0.086	0.084	0.049
	R^2	0.988	0.987	0.985	0.989	0.985	0.991
Pseudo-second-order	q_e(mg/g)	0.845	1.046	1.182	3.917	9.167	17.33
	K_2	0.014	0.043	0.059	0.029	0.014	0.003
	R^2	0.997	0.993	0.992	0.998	0.999	0.999
Elovich	a	0.065	0.133	0.206	1.861	4.238	2.663
	T	4.049	4.178	4.253	1.461	0.639	0.249
	R^2	0.924	0.938	0.939	0.934	0.961	0.987
Two-constant	A	0.086	0.189	0.365	1.315	3.171	3.731
	b	0.495	0.358	0.303	0.227	0.222	0.331
	R^2	0.973	0.969	0.964	0.953	0.968	0.969
Intraparticle	$K_{int}1$	0.106	0.113	0.115	0.628	1.525	2.451
	$K_{int}2$	0.106	0.111	0.114	0.228	0.469	1.386
	$K_{int}3$	0.020	0.015	0.005	0.003	0.025	0.060
	R^2	0.993	0.982	0.970	0.989	0.982	0.976
Experimental	q_m Exp. (mg/g)	0.841	0.968	1.029	3.877	8.918	16.95

formation of inner-sphere complexes with thiol groups, which would enhance the monolayer adsorption capacity [7].

Adsorption kinetics

The adsorption kinetics parameters for the initial concentrations of 20, 50, and 100 mg/L are shown in Table 5. The adsorption kinetics are based on pseudo-first-order, pseudo-second-order, Elovich, Two-constant, and intraparticle diffusion kinetic models. Because the correlation coefficient $R^2 > 0.9$, the adsorption of Cd^{2+} on the two clays conformed to five kinetic models. The Elovich model explains that Bent possesses active heterogeneous surface sites such as Al_2O_3 and SiO_2 [46]. Bent may conform to this reaction mechanism as a result of complexation and electrostatic attraction between the positively charged ions (Cd^{2+}) in solution and negatively charged ions (–Si–O^- on the tetrahedral layers and –Al–O^- on the octahedral layers) on the bentonite surface or because Bent has a structural negative charge (permanent), which results in the presence of several interlayer exchangeable cations. Furthermore, the value of a may indicate chemisorption [47]. The R^2 value of SH-Bent was higher than that of Bent. The R^2 (approximately 1) of the

Table 6 Comparison of Cd^{2+} adsorption kinetics and isotherms with mineral-based adsorbents

Adsorbent	Optimum initial solution pH	Adsportion capacity (mg/g)	Adsorption isotherm model	Adsorption kinetic model	Reference
Ca-montmorillonite	4.8	20.03	Langmuir	Pseudo-second-order	[48]
Na-montmorillonite	7	17.61	Langmuir	Pseudo-second-order	[3]
Bentonite	6–8	8.20	Freundlich	Pseudo-second-order	[49]
Fe-montmorillonite	>7	25.70	Langmuir	Pseudo-second-order	[44]
Na-montmorillonite	>6.5	35.95	Langmuir	N.A	[50]
humic acid-montmorillonite	>8	97.6% (Removal rate)	Freundlich	Pseudo-second-order	[51]
Vermiculite	5	21.43	Langmuir	Pseudo-second-order	[52]

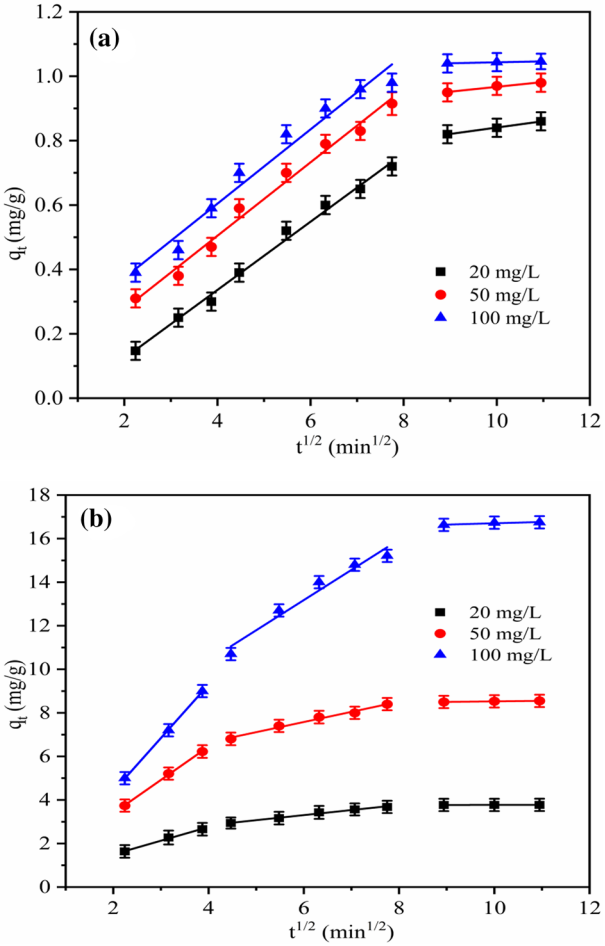

Fig. 8 Intraparticle diffusion plots for adsorption of Cd^{2+}on **a** Bent and **b** SH-Bent (adsorbent dose, 5 g/L; pH, 6.0 ± 0.1; contact time, 120 min; temperature, 30 ± 0.1 °C; 200 rpm)

pseudo-second-order model was the highest of all among the five adsorption kinetic models. The results better explained the experimental data. These results implied that the pseudo-second-order model was the best fit for the adsorption kinetic data. As shown in Table 6, the adsorption data of most minerals for Cd^{2+} were most consistent with the pseudo-second-order model description.

Moreover, the difference between Bent and SH-Bent can be compared using the intraparticle diffusion model. As shown in Fig. 8, the intraparticle diffusion plots of SH-Bent can be divided into three stages. There is a pronounced slope in the first stage, a gradual slope in the second stage, and almost no slope in the third stage. However, the plots for Bent can be divided into two stages, with a pronounced slope in the first stage and no slope in the second stage. Based on this model, the first part represents the external surface adsorption or instantaneous adsorption stage, which mostly involves a

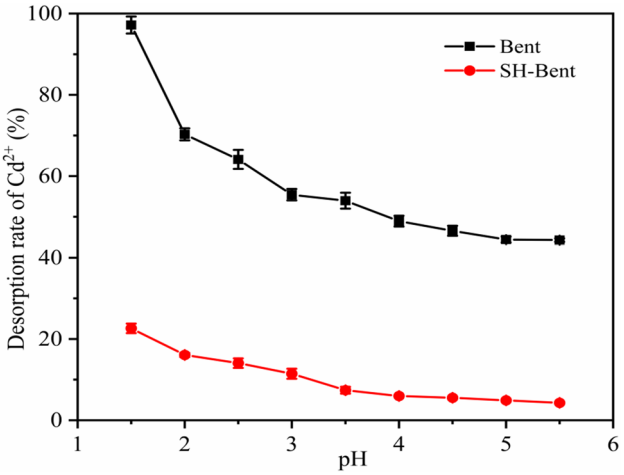

Fig. 9 Effect of pH on Cd^{2+} desorption on Bent and SH-Bent (adsorbent dose, 5 g/L; temperature, 30 ± 0.1 °C; 200 rpm; contact time, 60 min)

cation exchange mechanism [53, 54]. The second portion was ascribed to the gradual adsorption stage, in which the intraparticle diffusion was rate-controlled. The final linear portion represents the final equilibrium phase, during which the intraparticle diffusion rate decreased because of the low solute concentration. Therefore, the intraparticle diffusion data are consistent with what is known about the adsorption of Cd^{2+} on SH-Bent. Intraparticle diffusion occurred as a result of the smaller interlayer and tighter layered structures, which decreased the chance of external mass transfer and increased the chance of internal mass transfer [20]. For Bent, the first and second stages could be considered one, as the differences between their slopes, $K_{int}1$ and $K_{int}2$, were negligible (Table 5). Intraparticle diffusion proceeded smoothly due to the larger interlayer distance and external surface. These results differed from those reported by Ijagbemi [55], who believed that the second step was negligible.

Desorption studies in acid rain

Effect of the acid rain pH value

In the simulated acid rain system, the desorption rates of cadmium adsorbed by Bent and SH-Bent decreased as the pH increased from 1.5 to 5.5 (Fig. 9), which suggests that some of the H^+ probably interacted with the Cd^{2+} adsorbed on the adsorbent by ion exchange at lower pH [56]. In addition, the affinity of Cd^{2+} for the two absorbents was closely related to the pH, the competitive effect of protons on the adsorption site, and the reaction sites that were available due to the release of acid [57]. Figure 9 shows that the desorption rate of SH-Bent for cadmium in the presence of acid rain was much lower than that of Bent, which may be attributable to the formation of -S-Cd and the difficulty of Cd^{2+} desorption. Furthermore, for SH-Bent, the desorption rate of cadmium tends to balance when the acid rain pH was 3.5. It was

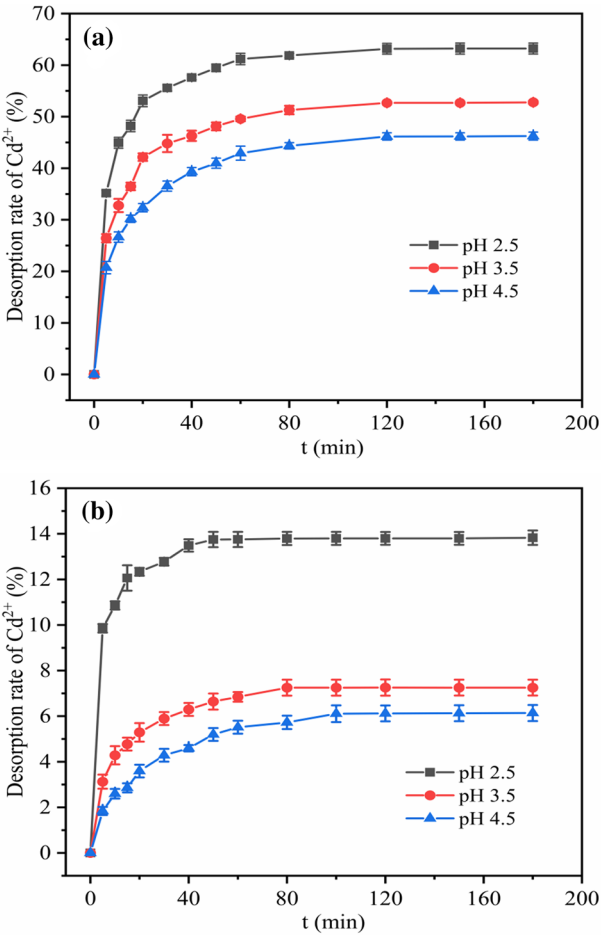

Fig. 10 Effect of desorption time of Cd^{2+} on **a** Bent and **b** SH-Bent (adsorbent dose, 5 g/L; temperature, 30 ± 0.1 °C; 200 rpm; contact time, 60 min)

proposed that SH-Bent was relatively stable for Cd^{2+} adsorption under natural conditions because pH values below 3.5 are infrequent in the natural environment [58].

Effect of desorption time

Figure 10 shows the results of three different pH treatments, indicating that the desorption capacity of cadmium begins to increase and subsequently stabilizes with an extended contact time, over two stages (fast and slow). Moreover, the two absorbents reached equilibrium within 60 min. The maximum desorption rates of Bent were 62.46, 52.58, and 45.68%, and those of SH-Bent were 13.24, 6.81, and 5.73% at pH 2.5, 3.5, and 4.5, respectively, which implied that the adsorption of cadmium by SH-Bent was more stable.

Table 7 Parameters of Kinetic model for the desorption of Cd^{2+} on Bent and SH-Bent

Sample	pH	Q_eExp(mg/g)	Pseudo-first-order			Pseudo-second-order			Elovich		
			Q_e(mg/g)	k_1	R^2	Q_e(mg/g)	k_2	R^2	a	τ	R^2
Bent	2.5	0.643	0.616	0.1321	0.969	0.662	0.3282	0.998	1.964	12.43	0.957
	3.5	0.541	0.512	0.0993	0.957	0.560	0.2683	0.994	0.462	12.26	0.982
	4.5	0.470	0.445	0.0795	0.954	0.493	0.2327	0.993	0.211	12.61	0.981
SH-Bent	2.5	4.989	4.857	0.2084	0.969	5.096	0.0794	0.996	1.096	2.386	0.917
	3.5	2.559	2.498	0.0767	0.972	2.561	0.0407	0.995	1.086	2.224	0.966
	4.5	2.160	2.026	0.0437	0.983	2.163	0.0219	0.992	0.804	2.078	0.961

Desorption kinetics

Cd^{2+} desorption data were calculated using pseudo-first-order, pseudo-second-order, and Elovich models. Table 7 lists the desorption kinetics parameters for the three kinetic models. The correlation coefficient was highest for the pseudo-second-order chemical reaction ($R^2 > 0.99$), which means that this model best describes the desorption of Cd^{2+} from Bent and SH-Bent. Furthermore, the Q_e values calculated using the pseudo-second-order model agreed well with the experimental data. Table 7 also shows that the desorption rate constants, k, of SH-Bent and Bent increased with the acidity of the inflow liquid, which indicates an increase in the desorption rate of Cd^{2+}. In addition, the desorption rate constant of SH-Bent was much lower than that of Bent under every pH condition tested, indicating that SH-Bent was not easily resolved and that the binding sites were strong (-S-Cd).

Conclusions

SH-Bent with cysteamine hydrochloride, a new material with a high Cd^{2+} removal capability, was prepared by the solution method. The maximum adsorption capacity of Cd^{2+} on SH-Bent calculated using the Langmuir isotherm model was 42-fold that of Bent, and the desorption rate of SH-Bent was much lower than that of Bent in simulated acid rain. The -S-Cd complexes formed by the specific binding of thiol groups in SH-Bent to Cd^{2+} are the key reason for these improvements. The results of this study indicate that SH-Bent is highly efficient and exhibits a low desorption rate for Cd^{2+}, and may provide foundational data for applications in wastewater treatment and the remediation of heavy metal-contaminated soil.

Acknowledgements The authors are thankful for the financial support of the Guizhou Provincial Science and Technology Foundation (No. 20201Y182).

Author contributions HQ and CL involved in conceptualization and methodology; RS took part in validation, investigation, writing—original draft; ZL and WL involved in software;YA and ML took part in resources; RS and HQ involved in writing—review & editing.

Declarations

Conflict of interest The authors declare that they have no conflict of interest. The authors declare that they have no known competing financial interests or personal relationships that could have appeared to influence the work reported in this paper.

References

1. L. Yao, L. Zhang, R. Wang, J. Hazard. Mater. **301**, 462 (2016)
2. X.L. Zhao, T. Jiang, B. Du, Chemosphere **99**(3), 41 (2014)

3. Z. Shen, X. Fan, D. Hou, F. Jin, Chemosphere **233**, 149 (2019)
4. H.B. Hadjltaief, A. Sdiri, W. Ltaief, C. R. Chimie. **21**(3–4), 253 (2018)
5. C. Chen, H. Liu, T. Chen, D. Chen, Appl. Clay Sci. **118**, 239 (2015)
6. N. Karapinar, R. Donat, Desalination **249**(1), 123 (2009)
7. L. Tran, P. Wu, Y. Zhu, S. Liu, N. Zhu, Appl. Surf. Sci. **356**(30), 91 (2015)
8. A. Gil, L. Santamaría, S.A. Korili, J. Environ. Chem. Eng. **9**(5), 105808 (2021)
9. M. Ghiaci, M.E. Sedaghat, H. Aghaeia, A. Gil, J. Chem. Technol. Biot. **84**(12), 1908 (2010)
10. D.Z. Rahman, J. Vijayaraghavan, J. Thivya, Biomass. Convers. Bior. **2**, 1 (2021)
11. L. Nie, P. Chang, S. Liang, C. Eng. Technol. **4**, 100167 (2021)
12. Y. Nuhoğlu, Z.E. Kul, S. Kul, Int. J. Environ. Sci. Te. **2**, 2975 (2021)
13. K.G. Bhattacharyya, S.S. Gupta, Desalination **272**(1–3), 66 (2011)
14. V.E. Anjos, J.R. Rohwedder, S. Cadore, Appl. Clay Sci. **99**, 289 (2014)
15. F.H. Nascimento, J.C. Masini, J. Environ. Manage. **143**, 1 (2014)
16. J.K. Guo, L. Wang, Y.L. Tu, J. Environ. Chem. Eng. **9**, 10663 (2021)
17. E. Eren, J. Hazard. Mater. **165**(1–3), 63 (2009)
18. Y. Wang, S. Li, H. Yang, J. Soil Sediment. **19**(15), 1767 (2019)
19. T.S. Anirudhan, M. Ramachandran, J. Colloid Interf. Sci. **299**(1), 116 (2006)
20. Y. Liu, M. Gao, Z. Gu, J. Hazard. Mater. **267**, 71 (2014)
21. M. Ghiaci, H. Aghaeia, Appl. Clay Sci. **43**(3–4), 289 (2009)
22. M. Ghiaci, H. Aghaeia, Appl. Clay Sci. **43**(3–4), 308 (2009)
23. M.E. Sedaghat, M. Ghiaci, H. Aghaei, Appl. Clay Sci. **46**(2), 125 (2009)
24. Y. Wang, T. He, D. Yin, Ecotox. Environ. Safe. **204**, 111121 (2020)
25. Y. Fei, C. Liu, F. Li, J. Geochem. Explor. **176**, 2 (2017)
26. V.P. Dinh, M.D. Ngugen, Chemosphere. **257**, 127147 (2020)
27. H. Long, P. Wu, N. Zhu, Chem. Eng. J. **225**, 237 (2013)
28. D.A. Skoog, *Principles of Instrumental Analysis*, 7th edn. (Cengage Learning, Boston, 2018), p. 287
29. V.P. Dinh, P.T. Ngugen, Chemosphere **266**, 131766 (2021)
30. S. Li, P. Wu, J. Hazard. Mater. **173**(1–3), 62 (2010)
31. X. Ni, Z. Li, Y. Wang, Front. Chem. **6**, 390 (2018)
32. R. Hua, Z. Li, Chem. Eng. J. **249**, 189 (2014)
33. E. Zolotoyabko, *Basic Concepts of X-ray Diffraction*, 1st edn. (John Wiley & Sons, Germany, 2014), p. 435
34. R. Guinebretiere, X-ray Diffraction by Polycrystalline Materials, 1st edn. (John Wiley Professio, London, 2007), pp. 345
35. U. Kuila, M. Prasad, Geophys. Prospect. **61**(2), 341 (2013)
36. D. Qin, X. Niu, M. Qiao, G. Liu, H. Li, Appl. Surf. Sci. **333**, 170 (2015)
37. J. Fan, C. Cai, J. Hazard. Mater. **388**, 122037 (2020)
38. J. Vijayaraghavan, D. Zunaithur Rahman, J. Thivya, Desalin. Water. Treat. **209**, 254 (2021)
39. Z. Zhu, C. Gao, Y. Wu, L. Sun, Bioresource Technol. **147**, 378 (2013)
40. J.A. Dean, Lange's Handbook of Chemistry, 15th edn. (McGraw-Hill, America, 1999)
41. K.O. Adebowale, I.E. Unuabonah, B.I. Olu-Owolabi, J. Hazard. Mater. **134**(1–3), 130 (2006)
42. K.G. Bhattacharyya, S.S. Gupta, Adv. Colloids Interface Sci. **140**, 114 (2008)
43. L.A.S.J. Carvalho, R.A. Konzen, A.C.M. Cunha, J. Environ. Chem. Eng. **7**(6), 103496 (2019)
44. P. Wu, W. Wu, S. Li, N. Xing, J. Hazard. Mater. **169**(1–3), 824 (2009)
45. H. Lui, X. Zhu, M. Han, Nonmetallic Ores. **36**(3), 4 (2013)
46. G.A. Neves, Materials. **14**, 5688 (2021)
47. D.D. Giri, J.M. Jha, A.K. Tiwari, Environ. Pollut. **280**(1), 116890 (2021)
48. L.D. Pablo, M.L. Chávez, M. Abatal, Chem. Engin. J. **171**(3), 1276 (2011)
49. B. Nagwa, S. Mahmoud, Minerals **6**(4), 129 (2016)
50. M. Stefan, D.S. Stefan, Rev. Chim. **60**, 1169 (2009)
51. L. Wang, X. Li, D.C.W. Tsang, F. Jin, J. Hazard. Mater. **387**, 2200510 (2020)
52. Y. Liu, H. Li, X.H. Zhu, Sep. Sci. Technol. **45**(2), 277 (2010)
53. S. Wang, W. Lao, RSC Adv. **11**, 35673 (2021)
54. S.M. Dal Bosco, R.S. Jimenez, Adsorption **12**(2), 133 (2006)
55. C.O. Ijagbemi, M. Baek, D.S. Kim, J. Hazard. Mater. **174**(1–3), 746 (2010)
56. D. Wang, X. Jiang, W. Rao, Ecol. Complex. **6**(4), 432 (2009)

57. V. Masindi, W.M. Gitari, J. Clean Prod. **112**(1), 1077 (2016)
58. W. Liu, C. Zhao, S. Wang, Res. Chem. Intermed. **44**(3), 1441 (2017)